Available online at www.sciencedirect.com

ScienceDirect

Journal of Magnesium and Alloys 10 (2022) 3447–3458

www.elsevier.com/locate/jma

Full Length Article

Extrusion limit diagram of AZ91–0.9Ca–0.6Y–0.5MM alloy and effects of extrusion parameters on its microstructure and mechanical properties

Dong Hee Lee[a], Ye Jin Kim[a], Sang-Hoon Kim[b], Byoung Gi Moon[c], Sung Hyuk Park[a,*]

[a] School of Materials Science and Engineering, Kyungpook National University, Daegu 41566, Republic of Korea
[b] Agency for Defense Development, Daejeon 34186, Republic of Korea
[c] Advanced Metals Division, Korea Institute of Materials Science, Changwon 51508, Republic of Korea

Received 7 January 2021; received in revised form 2 June 2021; accepted 4 June 2021
Available online 28 July 2021

Abstract

An AZ91–0.9Ca–0.6Y–0.5MM (AZXWMM91100) alloy, which has higher corrosion resistance, ignition resistance, and extrudability than a commercial AZ91 alloy, has been developed recently. In this study, the AZXWMM91100 alloy is extruded at various temperatures (300–400 °C) and ram speeds (1–14.5 mm/s), and the cracking behaviors, microstructure, and tensile properties of the extruded materials are systematically analyzed. On the basis of the pressure limit and surface and internal cracking limit, the extrusion limit diagram providing a safe extrusion processing zone is established. All of the materials extruded at temperatures and speeds within the safe extrusion processing zone have high surface quality and moderate tensile ductility with an elongation higher than 10%. Moreover, they have a fully recrystallized grain structure and contain undissolved particle stringers arranged parallel to the extrusion direction. The grain size of the extruded material does not show any relationship with the Zener–Hollomon parameter (Z). However, the yield strength (YS) of the extruded material is inversely proportional to the logarithm of the Z value, and their relationship is expressed as $YS = -31.2 \cdot \log(Z) + 536$. These findings may broaden the understanding of the AZXWMM91100 alloy with excellent chemical and physical properties and provide valuable information for the development of high-performance extruded Mg products using this alloy.

Keywords: Magnesium; Extrudability; Extrusion limit diagram; Microstructure; Tensile properties.

1. Introduction

International environmental regulations on the carbon dioxide emissions and fuel efficiency of vehicles are becoming increasingly stringent in response to the increasingly evident adverse effects of global warming. The weight reduction of automobiles has become an essential and urgent social task in such a scenario; consequently, Mg alloys have attracted considerable attention as a means to achieve such reduction via replacement of Fe- or Al-based components with those based on Mg [1–3]. Although Mg has the lowest density among commercial structural metals such as Fe, Ti, Al, and Cu, the widespread application of Mg alloys in the automobile industry is hindered by their inherent limitations, such as their rapid corrosion rate and easy ignition. Mg has a lower Gibbs free energy for oxidation compared with Fe and Al, which indicates that Mg alloys are thermodynamically more susceptible to oxidation than steels and Al alloys [4]. According to the classic Pilling–Bedworth (PB) rule, when the PB ratio—defined as the ratio of the molar volume of a metal oxide to the molar volume of the corresponding metal—is less than 1, the oxide is inclined to crack and will not provide any protection to the metal substrate [5]. Because the PB ratio of MgO, which is generally formed in commercial Mg alloys, is 0.81 [6], oxygen in the atmosphere easily penetrates the MgO layer and comes into contact with the base metal; this contact causes corrosion of bulk Mg alloys and ignition of molten

* Corresponding author.
E-mail address: sh.park@knu.ac.kr (S.H. Park).

https://doi.org/10.1016/j.jma.2021.06.002

Mg alloys. Furthermore, because Mg has the lowest negative standard potential among industrial metals, when Mg alloys are in contact with other metals, they corrode easily through the formation of a galvanic cell at the interface [7]. Commercial Mg alloys therefore have low corrosion and ignition resistances, and these characteristics limit their application to exterior components of automobiles.

Several studies have recently demonstrated that the combined addition of small amounts of Ca and Y (<1.0 wt% each) to commercial Mg–Al-based alloys significantly improves both the corrosion resistance and the ignition resistance of the alloys [8–12]. Go et al. [11] showed that when 0.3 wt% Ca and 0.2 wt% Y were added to an AZ80 alloy, its ignition temperature increased substantially by 220 °C (from 600 °C to 820 °C) because of the formation of dense double-layered protective oxides on the surface of the molten alloy. Baek et al. [12] reported that the addition of 0.25 wt% Y to an AZ61–0.5Ca alloy greatly decreased the corrosion rate of the alloy from 1.84 mm/y to 0.31 mm/y; this remarkable improvement in the corrosion resistance was attributed to the formation of the Al_8Mn_4Y or Al_2Y phase instead of the Al_8Mn_5 phase. Therefore, these Mg–Al–Zn–Ca–Y (AZXW) alloys, having excellent ignition and corrosion resistances, are expected to be widely applicable in various structural components of automobiles, high-speed trains, and aircraft that require weight reduction. Because wrought Mg materials have substantially higher mechanical properties than their cast counterparts, metal forming of AZXW alloys has been studied extensively in recent years [11,13–16]. Among the various metal forming processes, extrusion can afford products of various shapes (e.g., sheets, plates, beams, rods, and tubes) through only single-pass operation, unlike the rolling process, which generally requires several rolling passes and intermediate heat treatments [17,18]. However, two factors may restrict the extrusion of metallic materials: (i) the pressure limit, which is governed by the inherent stiffness of the material and the pressure capacity of the extrusion press, and (ii) the cracking limit, which is governed by incipient melting and which causes surface cracking of extruded products [19]. At low billet temperatures, the pressure limit occurs when the stress required to cause plastic flow of a material becomes equal to the maximum pressure capacity of the extrusion press. At high billet temperatures, the cracking limit occurs when the local temperature near the die land area exceeds the solidus temperature of a material or the melting temperature of second phases in the material. Accordingly, to obtain high-quality extruded products, it is necessary to carefully control the process conditions such that neither the pressure limit nor the cracking limit occurs during hot extrusion. To this end, safe extrusion process conditions for commercial Mg alloys such as AZ31, AZ61, and ZK60 have been established and employed at industrial sites [20].

Extensive efforts have been made to increase the maximum extrusion speed of Mg alloys with the aim of improving the extrusion process efficiency and productivity and enabling hot extrusion under more diverse process conditions [21–23]. However, as is the case with commercial AZ alloys, high-Al-containing AZXW alloys have considerably lower extrudability than commercial Al alloys; the maximum ram speed of an AZ91–0.9Ca–0.6Y (AZXW9110) alloy is only 2 mm/s at 350 °C [24]. In our previous study [24], a trace amount (0.5 wt%) of Ce-rich mischmetal (MM) was added to the AZXW9110 alloy to overcome its poor extrudability, and consequently, the maximum ram speed improved drastically, from 2 mm/s to 12 mm/s (i.e., a six-fold increase); this improvement was attributed to an increase in the thermal stability of preexisting undissolved second-phase particles. Therefore, this AZ91–0.9Ca–0.6Y–0.5MM (AZXWMM91100) alloy simultaneously has higher ignition resistance, corrosion resistance, and extrudability than commercial high-Al-containing Mg alloys (e.g., AZ80 and AZ91). Although the construction of the extrusion limit diagram of this alloy is necessary for ensuring its industrial applicability, no in-depth studies have yet been conducted to determine its pressure and cracking limits and its optimum extrusion conditions. In this study, therefore, an extrusion limit diagram containing a safe extrusion processing zone is constructed for the AZXWMM91100 alloy on the basis of the surface conditions, microstructural characteristics, and tensile properties of materials fabricated at various extrusion temperatures and ram speeds. In addition, the effects of the extrusion process parameters on the occurrence of several types of cracking during extrusion and on the microstructure and tensile properties of the extruded material are investigated and the relationship between the extrusion conditions and the corresponding mechanical properties is determined.

2. Experimental procedure

2.1. Materials

A Mg–9Al–0.8Zn–0.9Ca–0.6Y–0.5MM (AZXWMM 91100, wt%) alloy was used in this study. Billets for extrusion were prepared by the following procedure. (i) A graphite crucible with a diameter of 97 mm and a length of 200 mm was placed in an electric resistance furnace. (ii) Commercial AZ91 alloy ingots were placed in the graphite crucible and then melted at 720 °C under a protective atmosphere containing a CO_2–SF_6 (10:1) gas mixture. (iii) Mg–20Ca (wt%) and Mg–30Y (wt%) master alloys, pure Al granules, and MM granules were added to the molten AZ91 alloy. (iv) The resultant molten metal was held at 850 °C for 30 min to stabilize it and then stirred carefully to ensure homogeneity of the chemical composition. (v) The molten metal was poured at 750 °C into a steel mold preheated to 210 °C, with dimensions of 80 mm (diameter) × 170 mm (length). The approximate chemical composition of the MM used in this study was 75 wt% Ce + 25 wt% La and the master alloys were purchased from Hunan China Company. The cast billets were subjected to homogenization heat treatment at 445 °C for 24 h in an electric furnace and then water-quenched.

2.2. Hot extrusion

Cylindrical samples (70 mm diameter × 120 mm length) were machined from the homogenized billets for use in hot extrusion. The machined samples were preheated to target extrusion temperatures of 300, 325, 350, and 400 °C in an electric furnace and then subjected to direct extrusion with an extrusion ratio of 22.9 at various ram speeds in the following combinations: 1 mm/s and 4 mm/s at 300 °C; 1, 4, 7, 10, 12, and 14.5 mm/s at 325 °C; 1, 4, 6, 7, 10, 12, and 14.5 mm/s at 350 °C; and 1, 2, 3, and 4 mm/s at 400 °C. A horizontal-type hydraulic extrusion machine with a maximum load capacity of 300 tons and a flat-faced die with a single rectangular hole (6 mm thick and 28 mm wide) was used for the direct hot extrusion experiments, and the resultant extruded sheets were naturally cooled down in air after they exited the extrusion die. During the entire extrusion process, the extrusion load and ram travel distance were automatically measured using the load cell and drive system of the extrusion machine.

2.3. Microstructural observations

Microstructures of the extruded materials were analyzed by optical microscopy (Olympus, JP/BX53) and field-emission scanning electron microscopy (FE-SEM; Hitachi, SU8230). The grain sizes of the extruded materials were measured by the linear intercept method. All specimens for microstructure observations were mechanically ground with progressively finer grades of emery paper (from #120 grit to #2000 grit) and then polished with 3 μm and 1 μm diamond pastes; they were subsequently subjected to a final polish with colloidal silica solution (0.04 μm) for 30 min to achieve a high-quality surface finish. The polished specimens were etched with an acetic-picral solution (1.5 g picric acid + 5 ml acetic acid + 5 ml distilled water + 50 ml ethyl alcohol), and their microstructures were observed on the extrusion direction (ED)–transverse direction (TD) plane.

2.4. Mechanical testing

For tensile tests, subsized flat dogbone-shaped specimens (gage dimensions: 25 mm (length) × 6 mm (width) × 3 mm (thickness)) were machined from the extruded materials in accordance with the ASTM E8M standard; the loading direction of these specimens was parallel to the ED. The tensile tests were performed using a Shimadzu AGS-100kNX universal testing machine at ambient temperature (23 °C) and a strain rate of 1×10^{-3} s^{-1}. Each extruded material was subjected to tensile testing three times to ensure repeatability of the tests and to verify the consistency of their results. The tensile properties of the extruded materials were determined by averaging the values obtained from the three tensile tests, and for simplicity, a representative curve for each extruded material was displayed. All the specimens for the microstructural analyses and tensile testing were extracted from the mid-thickness and mid-width sections of the extruded materials.

3. Results and discussion

3.1. Variation in extrusion load with temperature and ram speed

Fig. 1a–c shows the variations in the extrusion load during direct extrusion at the temperatures 325, 350, and 400 °C, respectively, with the ram speed. At all ram speeds, the extrusion load generated during extrusion at the temperature of 300 °C exceeds the load capacity of the employed extrusion machine. Hence, extrusion experiments cannot proceed at this temperature because the stress required to cause plastic flow of the material is higher than the pressure limit of the extruder. In extrusion experiments typically performed below the pressure limit, the extrusion load increases rapidly in the initial stage of extrusion until it reaches the maximum value; in this time period, the billet is plastically compressed in the container. The compressed billet begins to exit the extrusion die at the maximum extrusion load, and subsequently, the extrusion load decreases gradually as the extrusion proceeds further. Unlike in indirect extrusion, where friction occurs only between the billet and the die, in direct extrusion, friction also occurs between the billet and the container wall because the entire billet moves toward the die during extrusion [25]. Accordingly, as the billet exits the die during direct extrusion, the length of the billet remaining in the container shortens and, in turn, the friction between the billet and the container wall decreases; this consequently results in a gradual reduction in the extrusion load.

Fig. 1d shows the variation in the maximum extrusion load with the ram speed at each extrusion temperature. At a given ram speed, the maximum extrusion load decreases with increasing extrusion temperature because a higher temperature results in lower flow stress of a material. In addition, the flow stress of a material generally increases with increasing strain rate. An increase in the ram speed leads to an increase in the strain rate during extrusion, which consequently causes an increase in the extrusion load. In this study, as the ram speed increases from 1 mm/s to 14.5 mm/s, the maximum extrusion load increases from 286 tons to 305 tons at 325 °C and from 256 tons to 280 tons at 350 °C. At 400 °C, as the ram speed increases from 1 mm/s to 4 mm/s, the maximum extrusion load increases from 209 tons to 234 tons. The average increments in the maximum extrusion load caused by the increase in the ram speed are 1.31, 1.66, and 6.25 tons/(mm/s) at the extrusion temperatures of 325, 350, and 400 °C, respectively; that is, the degree of increase in the maximum extrusion load is large at higher temperatures. When the friction between the billet and the container wall is considered alone, the total extrusion pressure can be taken to be the sum of the die pressure and the pressure required to overcome the friction in the container (i.e., the frictional pressure) [26]. Because the coefficient of friction increases with increasing temperature, the increase in the frictional pressure caused by the increase in the ram speed becomes more pronounced at higher extrusion temperatures. Moreover, the strain rate dependence of the flow stress of a material increases with an increase in the deforma-

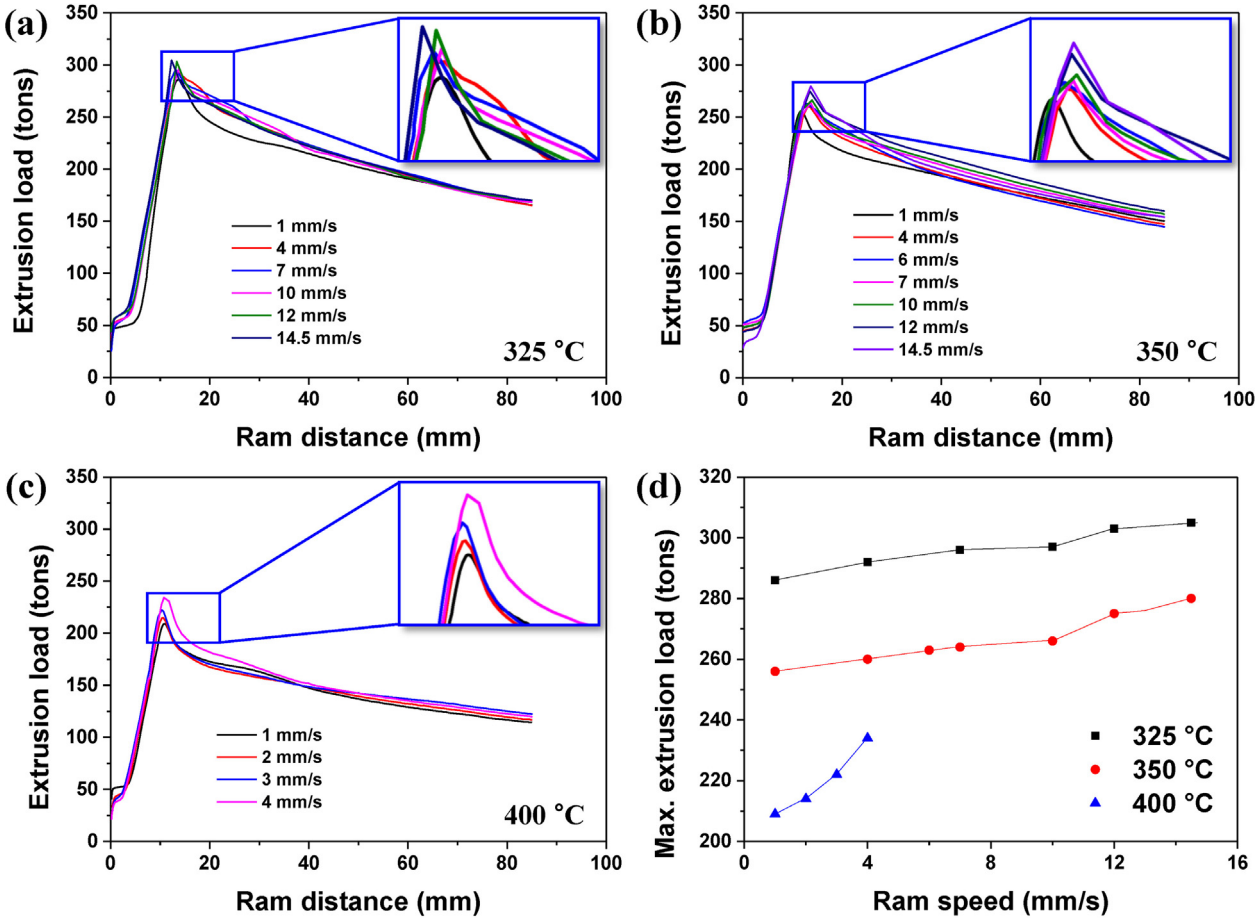

Fig. 1. (a–c) Variation in extrusion load during direct extrusion at various temperatures ((a) 325 °C, (b) 350 °C, and (c) 400 °C) with ram speed. (d) Variation in maximum extrusion load with ram speed.

tion temperature [27]; accordingly, even when the degree of increase in the strain rate remains the same, the increase in the flow stress at a higher temperature is larger than that at a lower temperature. Therefore, the sensitivity of the maximum extrusion load to the ram speed increases as the extrusion temperature increases, as shown in Fig. 1d.

3.2. Hot cracking during extrusion and maximum extrusion speed

Fig. 2 shows photographic images of the materials extruded at 325, 350, and 400 °C and various ram speeds. The three materials extruded at the ram speed of 1 mm/s have high-quality surfaces without any cracks, whereas those extruded at ram speeds in the range of 4–12 mm/s at 325 °C and 350 °C and those extruded at the ram speed of 2 mm/s at 400 °C contain numerous small cracks on both ED–ND planes. Moreover, in the material extruded at a high ram speed of 14.5 mm/s at 325 °C, hot cracking (involving formation of cracks larger than 15 mm) occurs in the direction perpendicular to the ED on the ED–TD plane. Hot cracking also occurs in the material extruded at the same ram speed of 14.5 mm/s at a higher temperature of 350 °C; however, the degree of this hot cracking is severer, which results in partial fracture of the extruded material. At the highest temperature of 400 °C, severe hot cracking occurs at the ram speed of 3 mm/s, which is much lower than the ram speed of 14.5 mm/s at which hot cracking occurs when the extrusion temperatures are 325 °C and 350 °C. Therefore, the maximum extrusion speed at which extrusion can be performed without hot cracking of the extruded material is 12 mm/s at 325 °C, 12 mm/s at 350 °C, and 2 mm/s at 400 °C; these results reveal that the extrudability of the AZXWMM91100 alloy is drastically lower at the highest extrusion temperature of 400 °C.

According to the equilibrium phase diagram of Mg–*x*Al–0.8Zn–0.9Ca–0.6Y (x = 0–15 wt%) calculated using PANDAT software, as the amount of Al added to a Mg–0.8Zn–0.9Ca–0.6Y alloy increases from 9.0 wt% to 11.3 wt%, the solidus temperature of this alloy decreases considerably from 456 °C to 426 °C [28]. In the case of a Mg–Al-based alloy, the concentration of Al solute atoms can be nonuniform even after homogenization treatment of the as-cast billet because considerable time is required for complete decomposition of the $Mg_{17}Al_{12}$ phases—which are locally formed in the interdendritic region and along the grain boundaries during solidification—and for homogeneous distribution of the decomposed Al atoms throughout the material via vol-

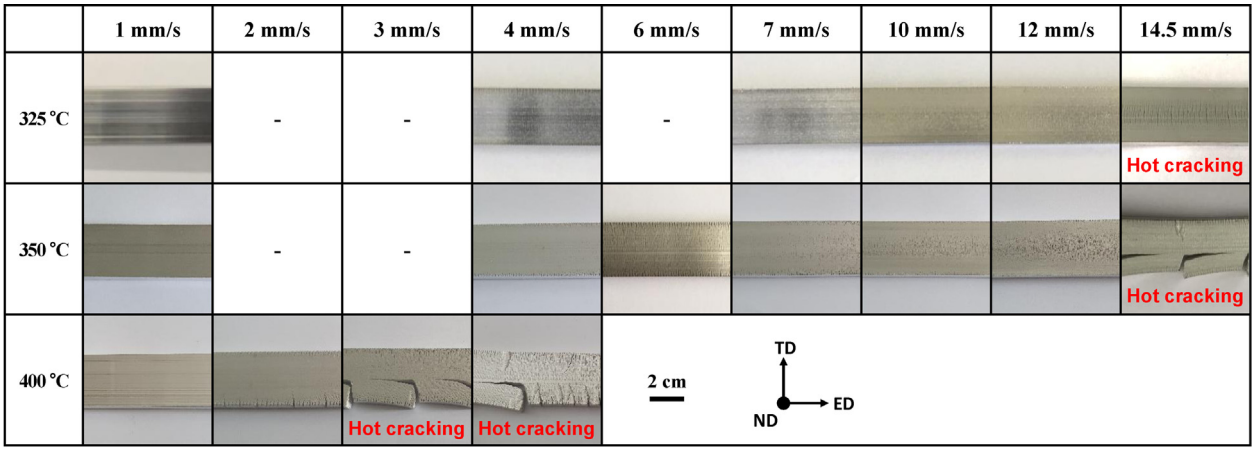

Fig. 2. Photographic images showing surface quality of AZXWMM91100 sheets extruded at various ram speeds and extrusion temperatures (325, 350, and 400 °C). Here, the length, width, and thickness of the extruded sheets are parallel to the extrusion direction (ED), transverse direction (TD), and normal direction (ND), respectively.

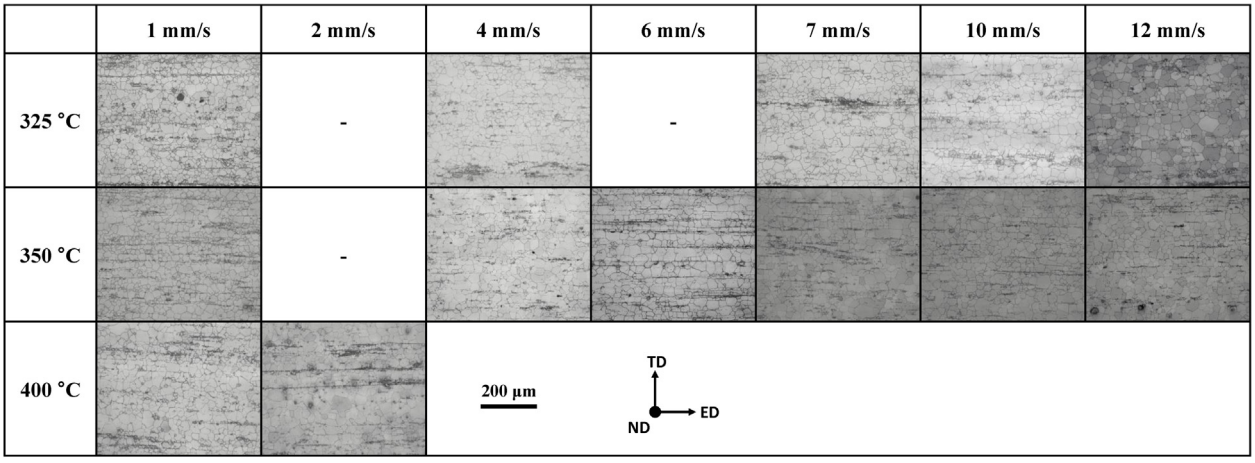

Fig. 3. Optical micrographs of extruded materials fabricated under extrusion conditions that do not induce hot cracking.

ume diffusion [29]. Therefore, the melting point of the local region with a higher Al concentration is lower than the solidus temperature of the alloy. Moreover, at a temperature lower than the solidus temperature of an alloy, a liquid phase generally nucleates at grain boundaries owing to their high free energy [30,31]. Therefore, it appears that even when the AZXWMM91100 alloy is extruded at a relatively low ram speed of 3 mm/s at 400 °C, local melting occurs in a region with high Al concentrations or at the grain boundaries during extrusion, and this melting eventually causes hot cracking because the local temperature in the die land area is higher than the melting points of these regions.

3.3. Variation in microstructure with extrusion temperature and ram speed

Microstructural observations and tensile tests were performed for the extruded materials that did not undergo hot cracking. Optical micrographs of the extruded materials are shown in Fig. 3, which reveal that all the extruded materials consist of equiaxed recrystallized grains and are devoid of elongated unrecrystallized grains. This observation suggests that when the AZXWMM91100 alloy is extruded at or above a temperature of 325 °C and a ram speed of at least 1 mm/s with an extrusion ratio of 22.9, complete dynamic recrystallization occurs during extrusion, and consequently, the extruded materials can have a uniform grain structure. Our previous study [24,28,32] showed that abundant undissolved Al_8Mn_4Y, Al_2Ca, and Al_2Y particles are present in the homogenized AZXWMM91100 billet and that they are rearranged along the ED during extrusion. Because these undissolved particles do not dissolve into the matrix during hot extrusion, all the extruded materials in the present study are observed to contain particles distributed parallel to the ED; that is, the presence of these observed particles is independent of the extrusion temperature and ram speed. As the extrusion temperature or ram speed increases, the size of recrystallized grains of the extruded material increases (Fig. 3); this tendency is consistent with previously reported results for extruded Mg alloys [33–39]. As the ram speed increases, the amount of heat generated by plastic deformation and friction during extrusion increases; consequently, the actual temper-

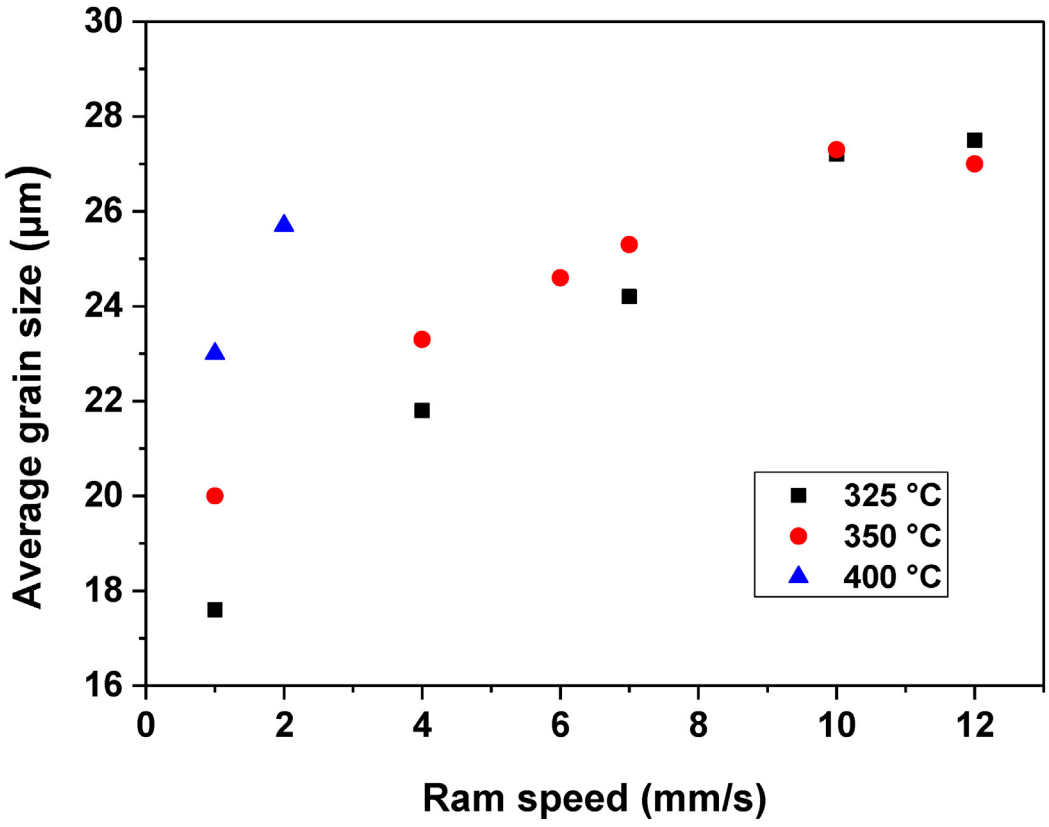

Fig. 4. Variations in average grain sizes of materials extruded at various temperatures with ram speed.

ature in the deformation zone increases with increasing ram speed [21,38–40]. Therefore, at a given extrusion temperature, an increase in the ram speed promotes the growth of recrystallized grains during extrusion because grain-boundary migration occurs faster at a higher temperature in the deformation zone.

Fig. 4 shows variations in the average grain size of the extruded materials with the ram speed and extrusion temperature. At a given extrusion temperature, the average grain size increases almost linearly with increasing ram speed; this is attributed to the promotion of grain coarsening with an increase in the deformation heat and friction heat. Several studies have examined the change in the grain size of extruded Mg alloys with the extrusion speed. For instance, Yu et al. [41] reported that the average size of recrystallized grains of an extruded ZK60 alloy increases significantly from 2.0 μm to 11.0 μm as the ram speed increases from 0.3 mm/s to 3 mm/s at an extrusion temperature of 250 °C. Further, the average grain size of an extruded Mg–7Sn–1Al–1Zn (TAZ711) alloy increases from 7.5 μm to 37.5 μm as the ram speed increases from 1 mm/s to 8 mm/s at an extrusion temperature of 350 °C [39]. Moreover, the average size of recrystallized grains of an extruded Mg–1Zn–1Mn–0.5Ce alloy increases greatly from 5.3 μm to 20.4 μm as the ram speed increases from 1 mm/s to 9 mm/s at an extruded temperature of 400 °C [38]. However, in the present study, although the ram speed increases considerably from 1 mm/s to 12 mm/s, the average grain size increases to a relatively small extent, from 17.6 μm to 27.5 μm at 325 °C and from 20.0 μm to 27.0 μm at 350 °C. That is, in the case of the AZXWMM91100 alloy, a 12-fold increase in the ram speed results in increments of only 35%–56% in the grain size of the extruded material, and these increments are substantially smaller than those in the grain sizes of the above-mentioned alloys (increments of 450%, 400%, and 285% for ZK60, TAZ711, and Mg–1Zn–1Mn–0.5Ce, respectively) even though the degree of increase in the ram speed for the former alloy (12-fold) is larger than those for the latter alloys (8–9-fold).

In addition, when the extrusion temperature increases from 325 °C to 400 °C at the ram speed of 1 mm/s, the average grain size of the AZXWMM91100 alloy increases only slightly, from 17.6 μm to 23.0 μm. This insignificant grain coarsening (i.e., the weak dependence of grain size on the extrusion speed and temperature) of the AZXWMM91100 alloy is a result of suppression of grain growth by the undissolved particles. Fig. 5 shows the optical and SEM micrographs of the material extruded at 350 °C and a high ram speed of 12 mm/s, as observed on the ED–TD plane. It can be seen that the undissolved particles are distributed in the form of stringers parallel to the ED and the grains adjacent to the particles do not grow beyond these particle stringers; this blocked grain growth is confirmed from the observation that the boundaries of these grains are formed parallel to the ED along the particle stringers. Therefore, when growing recrystallized grains meet the barrier-like particle stringers, subsequent growth of these grains becomes difficult; consequently,

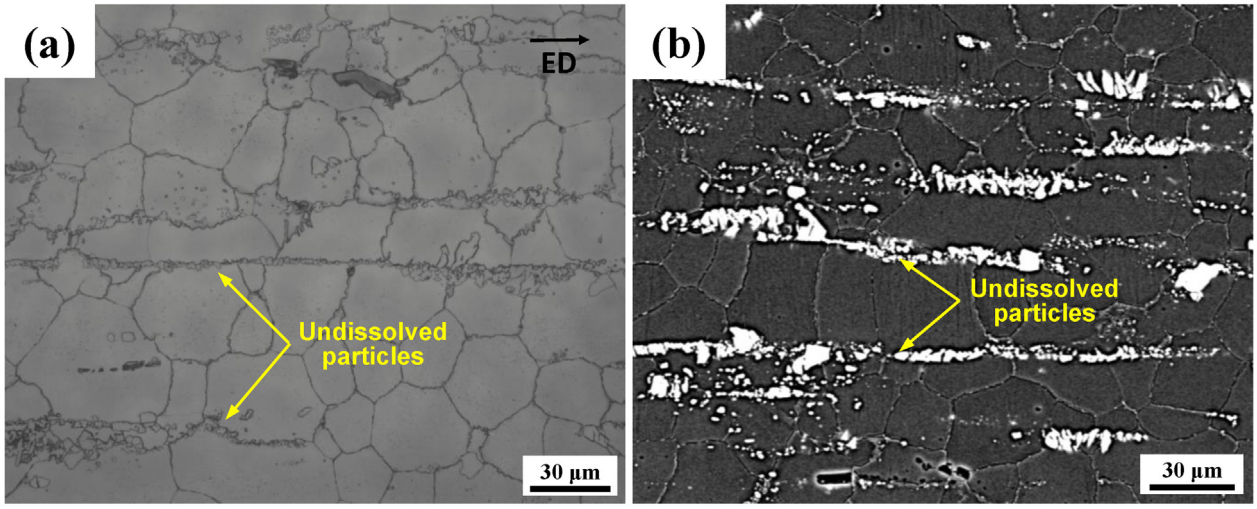

Fig. 5. (a) Optical and (b) SEM micrographs of material extruded at 350 °C and high ram speed of 12 mm/s.

Table 1
Process conditions of extrusion experiments and tensile properties and average grain sizes of extruded AZXWMM91100 materials.

Extrusion condition				Tensile properties**			Grain size (μm)
Temperature (°C)	Ram speed (mm/s)	Strain rate (s^{-1})	Z^* (s^{-1})	YS (MPa)	UTS (MPa)	EL (%)	
325	1	0.279	1.76×10^{11}	183 (±2.3)	303 (±4.1)	11.9 (±1.3)	17.6
	4	1.118	7.02×10^{11}	166 (±2.4)	304 (±0.4)	15.1 (±0.1)	21.8
	7	1.956	1.23×10^{12}	157 (±2.2)	288 (±8.7)	11.4 (±2.3)	24.2
	10	2.794	1.76×10^{12}	146 (±0.9)	251 (±6.5)	6.0 (±0.7)	27.2
	12	3.353	2.11×10^{12}	119 (±8.6)	170 (±12.0)	2.5 (±0.4)	27.5
350	1	0.279	5.90×10^{10}	205 (±3.3)	315 (±0.2)	13.0 (±1.2)	20.0
	4	1.118	2.36×10^{11}	182 (±0.9)	308 (±1.1)	15.1 (±0.4)	23.3
	6	1.677	3.54×10^{11}	176 (±0.6)	305 (±6.3)	11.3 (±1.6)	24.6
	7	1.956	4.13×10^{11}	165 (±2.9)	266 (±4.1)	7.2 (±0.6)	25.3
	10	2.794	5.90×10^{11}	125 (±3.3)	183 (±9.5)	2.9 (±0.5)	27.3
	12	3.353	7.08×10^{11}	96 (±12.0)	122 (±15.8)	1.2 (±0.3)	27.0
400	1	0.279	8.51×10^{9}	224 (±0.9)	327 (±6.0)	10.4 (±1.9)	23.0
	2	0.559	1.70×10^{10}	213 (±0.7)	323 (±3.6)	12.3 (±1.7)	25.7

* Z denotes the Zener–Hollomon parameter.
** YS, UTS, and EL denote the yield strength, ultimate tensile strength, and elongation, respectively.

excessive grain coarsening does not occur even at high ram speeds or high extrusion temperatures. In our previous study [28], we also found that when the AZXWMM91100 alloy and a commercial AZ91 alloy are extruded under the same extrusion conditions, the average grain size of the former is smaller than that of the latter because of the grain-boundary pinning effect induced by the undissolved particles in the former.

3.4. Tensile strength and elongation of extruded materials

Fig. 6 shows the engineering stress–strain curves of the extruded materials, and Table 1 lists the corresponding tensile properties. At all the extrusion temperatures, the yield strength (YS) and ultimate tensile strength (UTS) of the extruded material decrease with increasing ram speed, which is attributed mainly to the increase in the grain size. According to the Hall–Petch relationship, the YS of a material is proportional to the reciprocal of the square root of its grain size [42]. In this study, the volume fraction of grain boundaries—which act as obstacles to dislocation glide and cause them to pile up on their slip plane behind the boundaries—reduces with the coarsening of the recrystallized grains of the extruded material, and consequently, the YS of the extruded material decreases. All the as-cast billets used in this study have the same chemical composition and are subjected to the same homogenization treatment. Hence, the types and amounts of undissolved particles are identical in all the extruded materials; this suggests that the second-phase particle hardening induced by the undissolved particles is almost the same in all the extruded materials (that is, it is almost independent of the extrusion temperature and ram speed). It is well known that in extruded Mg alloys with a partially recrystallized grain structure, unrecrystallized grains have considerably higher dislocation densities than recrystallized grains because the former grains are continuously subjected to plastic deformation during the entire extrusion process [14,15,43]. In the present study, all the extruded materials consist of only recrystallized grains and are devoid of any unrecrys-

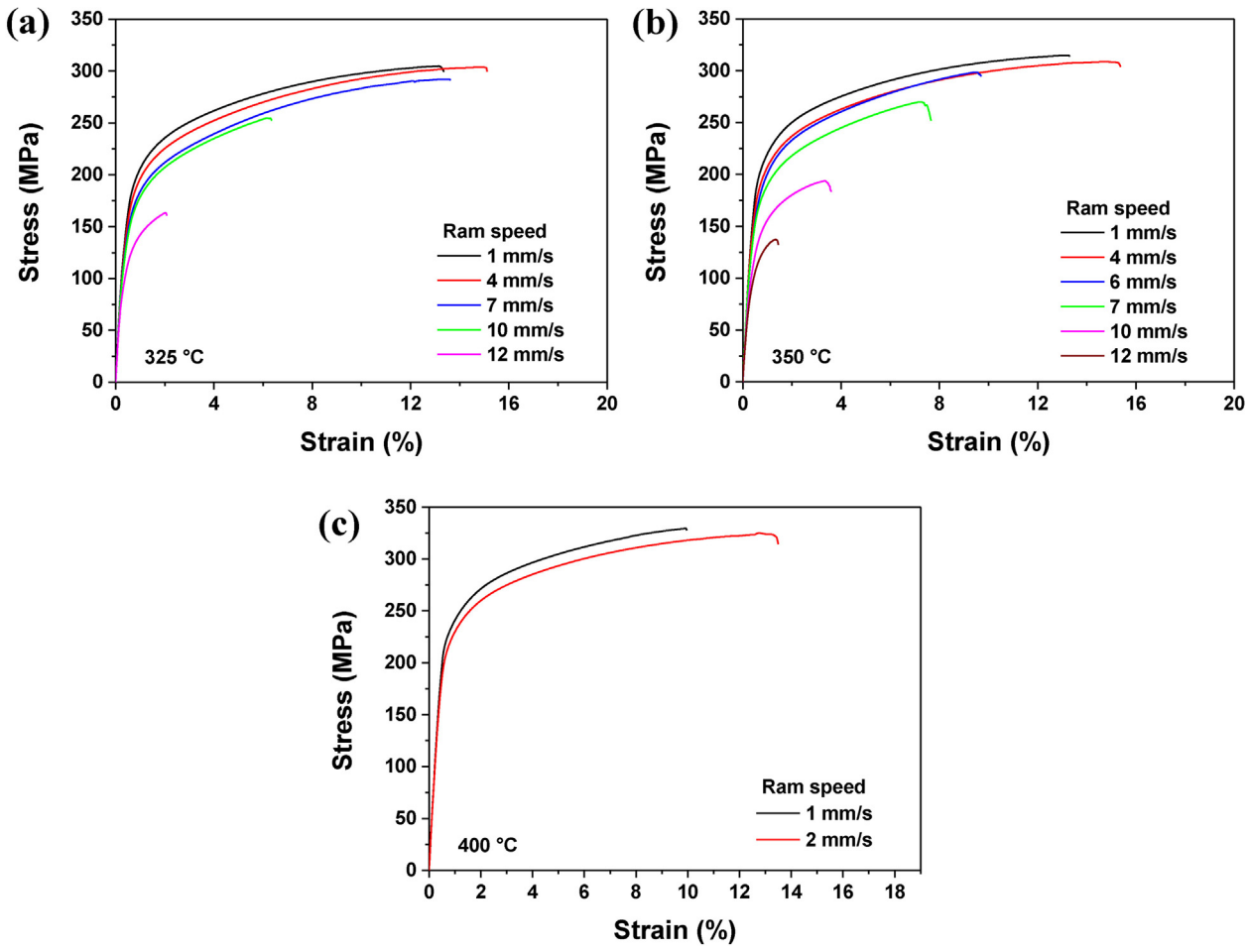

Fig. 6. Engineering tensile stress–strain curves of materials extruded at (a) 325 °C, (b) 350 °C, and (c) 400 °C.

tallized grains, and therefore, the strain hardening effect under tensile deformation is likely to be similar in all the materials.

Among all the tested materials, the material extruded at 400 °C and 1 mm/s has the highest YS (224 MPa) and that extruded at 350 °C and 12 mm/s has the lowest YS (96 MPa) (Table 1). In terms of ductility, the materials extruded at 325 °C and 350 °C at a ram speed of 4 mm/s have the highest tensile elongation (15.1%). It is notable that at the extrusion temperature of 325 °C, when the ram speed increases from 7 mm/s to 10 mm/s, both the UTS and the elongation of the extruded material decrease significantly, from 288 MPa to 251 MPa and from 11.4% to 6.0%, respectively (Fig. 6a and Table 1). Similarly, at the extrusion temperature of 350 °C, when the ram speed increases from 6 mm/s to 7 mm/s, both the UTS and the elongation decrease greatly, from 305 MPa to 266 MPa and from 11.3% to 7.2%, respectively (Fig. 6b and Table 1). Fig. 7 shows optical images on the ED–TD plane at the mid-thickness and mid-width of the unetched samples of two extruded materials (one extruded at 325 °C and 10 mm/s and the other extruded 350 °C and 7 mm/s) whose UTS and elongation deteriorate drastically. In both the materials, internal cracks longer than 20 μm are formed in a direction almost perpendicular to the ED (see the red arrows in Fig. 7a and b). As the deformation rate of a material increases, the degree of plastic instability increases and the residual stress in the material increases, both of which can lead to the formation of microcracks inside the deformed material [25,44]. Internal cracks with a size larger than the critical size easily propagate during tensile deformation because of the stress concentrated on them, and this, in turn, causes premature fracture. Therefore, when the AZXWMM91100 alloy is extruded under the temperature and ram speed conditions of (i) 325 °C and ≥10 mm/s or (ii) 350 °C and ≥7 mm/s, microsized internal cracks that cause drastic deterioration of the tensile properties are formed in the extruded material. For fabrication of an extruded AZXWMM91100 material free of undesirable internal cracks and having reliable mechanical properties, hot extrusion needs to be performed at a ram speed lower than the abovementioned ram speeds (10 mm/s at 325 °C and 7 mm/s at 350 °C).

3.5. Construction of extrusion limit diagram for AZXWMM91100 alloy

On the basis of the above-identified factors, i.e., the pressure limit, occurrence of cracking (hot, side, and internal), and tensile properties, an extrusion limit diagram of the

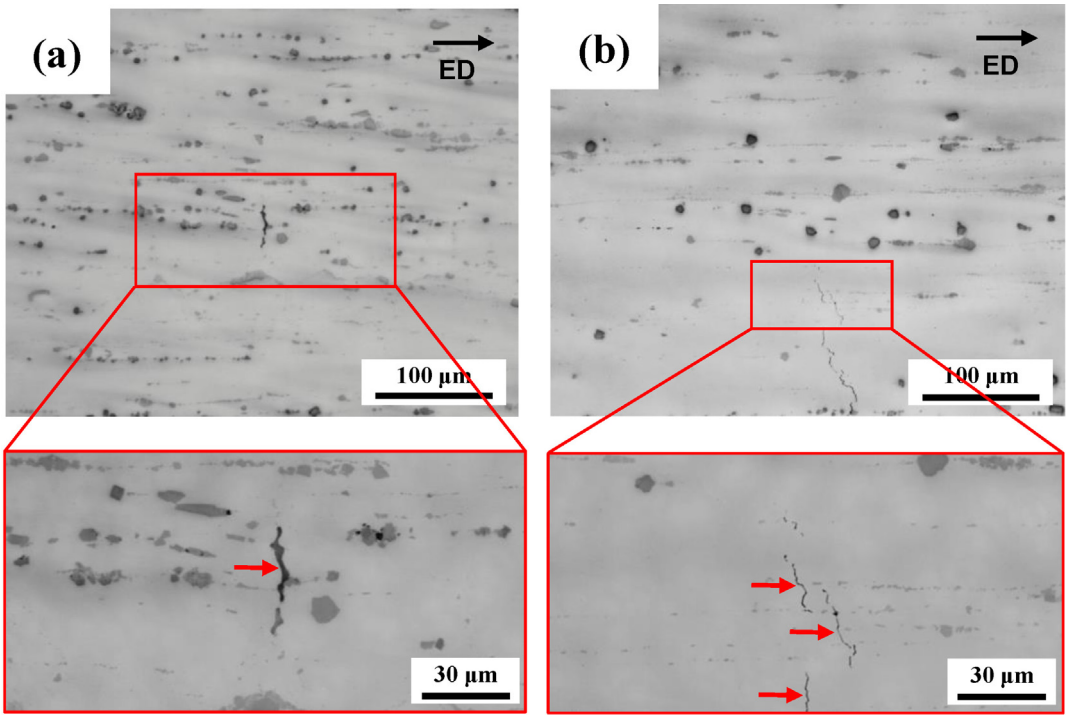

Fig. 7. Optical micrographs showing internal cracks formed in (a) material extruded at 325 °C and ram speed of 10 mm/s and (b) material extruded at 350 °C and ram speed of 7 mm/s.

AZXWMM91100 alloy is constructed by defining the safe extrusion processing zone (marked as "Safe zone" in Fig. 8) as the extrusion conditions that can provide a high-quality extruded material having a tensile elongation higher than 10% (Fig. 8). Extrusion conditions under which only side cracks are formed are included in the safe zone because small side cracks in the extruded material can be readily removed through milling to obtain high-surface-quality final products. However, if a material containing internal cracks is used as a structural component, then sudden fracture can occur during use through the activation of crack-accelerated fracture modes such as fatigue fracture, hydrogen-delayed fracture, and stress corrosion cracking. Hence, in this study, the extrusion conditions under which internal cracking occurs are excluded from the safe zone of the extrusion limit diagram. According to the constructed extrusion limit diagram of the AZXWMM91100 alloy, the allowable maximum ram speed is approximately 8 mm/s at 325 °C, 6 mm/s at 350 °C, 4 mm/s at 375 °C, and 2 mm/s at 400 °C, and the cracking limit line can be expressed as a function of ram speed (S) and extrusion temperature (T) as follows: $S = -0.081 \bullet T + 34.89$ (Fig. 8). As mentioned earlier, extrusion cannot be performed at 300 °C because the generated extrusion load is higher the maximum load capacity of the extrusion machine at this temperature. In this study, the diameter of the billet is 68 mm and the load capacity of the used extrusion machine is 300 tons; therefore, the available maximum pressure is calculated as 0.81 kN/mm^2. That is, the extrusion pressure generated at a relatively low extrusion temperature of 300 °C exceeds 0.81 kN/mm^2 before the material in the container exits the extrusion die, which makes the extrusion operation impossible. When structural components are manufactured using the AZXWMM91100 alloy in an actual extrusion plant, the size of the billet used is much larger than that used in the laboratory. For instance, when the direct extrusion process is performed using a large-sized billet with a diameter of 177.8 mm (7 in)—which is a widely used size in field-scale applications, direct extrusion at 300 °C using an extrusion machine having a maximum load capacity less than 2051 tons is found to be impossible owing to the occurrence of the pressure limit. It is considered that among the various extrusion conditions employed in this study, the extrusion condition of 350 °C and 4 mm/s is the optimum one under comprehensive consideration of the efficiency of extrusion processing (consumed energy and productivity) and the surface conditions and mechanical properties of the extruded material; the material extruded under this condition has the highest YS–elongation product of 2748 MPa•% among all the extruded materials.

3.6. Relationship between processing parameter and mechanical strength

The microstructure and resultant mechanical properties of a wrought metallic material subjected to hot forming are directly related to the process parameters, i.e., the strain, strain rate, and temperature. The strain applied during extrusion (ε) is determined using the extrusion ratio (ER) as follows [45]:

$$\varepsilon = ln(ER) \quad (1)$$

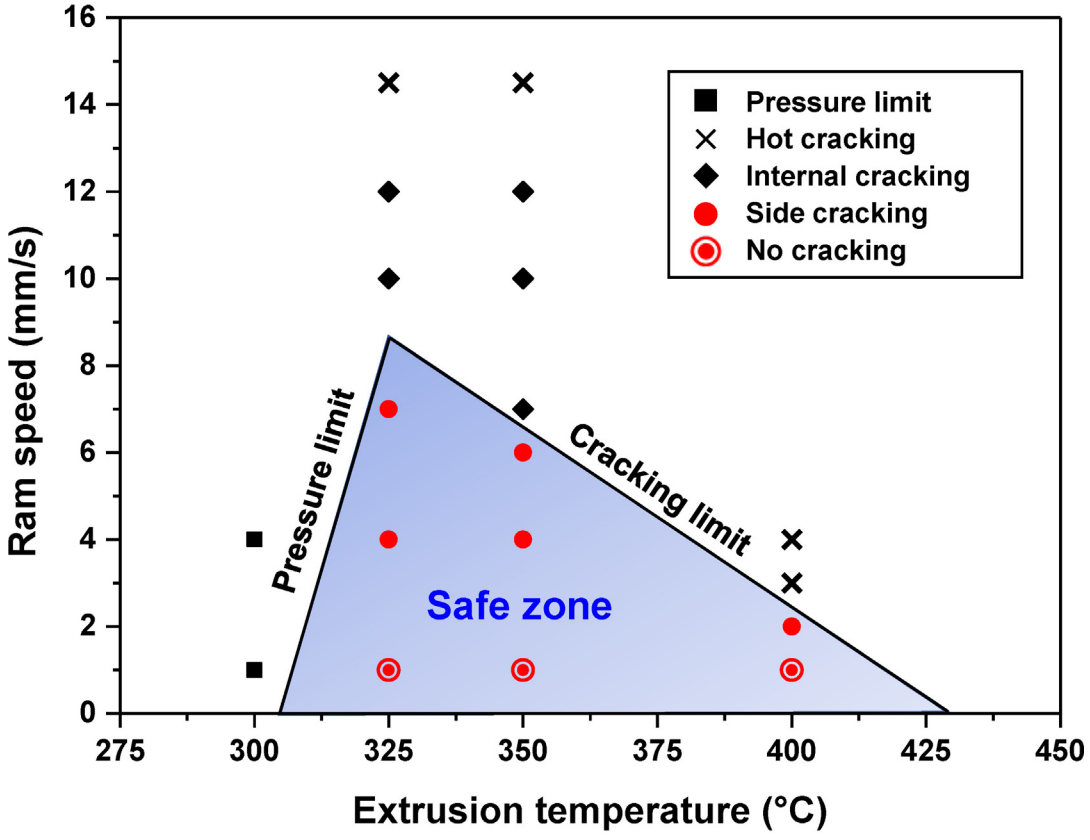

Fig. 8. Extrusion limit diagram of AZXWMM91100 alloy constructed on the basis of extrusion pressure and cracking limits.

Because all the extrusion experiments in this study are performed at the same extrusion ratio of 22.9, the same strain of 3.13 is applied during all the extrusion experiments; therefore, the process parameters influencing the microstructure and mechanical properties are the strain rate and temperature. The average strain rate during the extrusion process can be calculated using an equation proposed by Feltham [46]:

$$\bar{\dot{\varepsilon}} = \frac{6D_B^2 V_R \ln ER}{D_B^3 - D_E^3} \tag{2}$$

where V_R is the ram speed and D_B and D_E are the billet and extrudate diameters, respectively. In this study, the billet diameter, extrudate cross-sectional area, and extrusion ratio are the same under all the extrusion conditions; accordingly, the average strain rate varies only with the applied ram speed. In addition, the influence of both the strain rate ($\dot{\varepsilon}$) and the temperature (T) applied during hot forming can be expressed as a single value using the Zener–Hollomon parameter (Z) [47–50], which is defined as follows:

$$Z = \dot{\varepsilon} \exp\left(\frac{Q}{RT}\right) \tag{3}$$

where Q is the apparent activation energy of hot deformation, R is the universal gas constant (8.314 J/mol•K), and T is the deformation temperature (unit: Kelvin). During hot extrusion, plastic deformation of Mg alloys is predominantly governed by the glide and climb dislocations. Mirzadeh et al. [51–54] investigated the correlation between the flow stress during hot deformation and the Z value through constitutive analyses in various metallic materials. They found that when dislocation glide and climb are the main deformation mechanisms in Mg alloys, the lattice self-diffusion activation energy of Mg (135 kJ/mol) can be used as the hot deformation activation energy (Q) to calculate the Z value [51,52]. The average strain rate and Z value for each extrusion condition employed in this study are calculated using Eqs. (1)–(3) and listed in Table 1.

It is known that when a Mg alloy is subjected to homogeneous deformation at elevated temperatures in an isothermal atmosphere, the average size of recrystallized grains of the deformed alloy tends to be inversely proportional to the Z value [55]. However, in the extrusion process, in which high pressure and high strain are imposed on a material, the actual temperature in the deformation zone near the die differs greatly from the initial temperature, and this temperature difference is strongly dependent on the process parameters. For instance, when a TAZ711 alloy is extruded at a low temperature (250 °C) and high ram speed (8 mm/s), the temperature in the deformation zone increases significantly by 91 °C because of the heat generated by plastic deformation and friction [39]. In contrast, when the same alloy is extruded at a high temperature (400 °C) and low ram speed (0.1 mm/s), the temperature in the deformation zone decreases by 69 °C (i.e., cooling occurs during extrusion) because of the heat

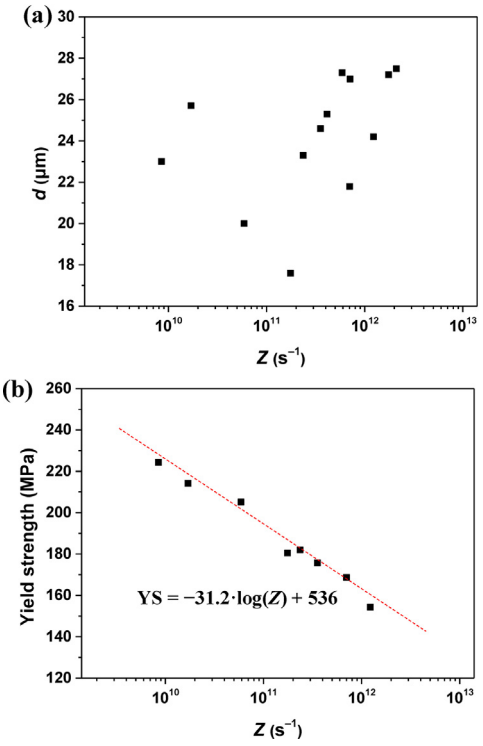

Fig. 9. Relationships between (a) Zener–Hollomon parameter (*Z*) and average grain size of extruded materials and (b) *Z* value and yield strength of extruded materials.

loss caused by heat transfer from the deforming material to the die and surroundings [39]. Because of such a considerable difference between the initial extrusion temperature and the actual deformation temperature, the abovementioned inverse relationship between the *Z* value and the grain size is generally not found to exist for extruded Mg alloys [38,39]. Cheng et al. [56] reported that when an exit extrusion temperature is used for calculating Z value instead of an initial extrusion temperature, the conventional inverse relationship between the *Z* value and the grain size is well established in extruded Mg alloys because the exit extrusion temperature is close to the actual temperature in the deformation zone. In this study, the *Z* values—which are derived from the initial process conditions—do not show any relationship with the grain sizes of the extruded materials—which are governed by metallurgical phenomena (e.g., recrystallization and grain coarsening) in the deformation zone (Fig. 9a). However, from a semilogarithmic graph with a linear vertical scale for the YS and a logarithmic horizontal scale for the *Z* value (Fig. 9b), it can be clearly seen that the YS of the extruded materials decreases linearly with increasing *Z*, and their relationship is expressed as $YS = -31.2 \cdot \log(Z) + 536$. Therefore, it is possible to produce an extruded material without internal cracking and hot cracking by using the constructed extrusion limit diagram. In addition, the strength of the extruded material processed within the safe zone of the extrusion limit diagram can be predicted simply using the established relational equation between the YS and the *Z* value, without having to perform extrusion and mechanical testing. We anticipate that all these findings of the present study will provide valuable information for the development of high-performance extruded Mg products using the recently developed AZXWMM91100 alloy, which has good corrosion and ignition resistances and enhanced extrudability.

4. Summary

In this study, we construct the extrusion limit diagram of the AZXWMM91100 alloy by performing direct extrusion at various temperatures and ram speeds and subsequently analyzing the extrusion load, surface conditions, microstructure, and mechanical properties of the extruded materials. The maximum extrusion load increases gradually with decreasing extrusion temperature and increasing ram speed. Extrusion does not proceed at 300 °C because at this temperature, the stress required to induce plastic flow of the material is higher than the pressure limit of the extrusion machine. When the applied ram speeds are higher than 10 mm/s and 7 mm/s at the extrusion temperatures of 325 °C and 350 °C, respectively, microsized internal cracks are formed in the material. In addition, severe hot cracking occurs at ram speeds of 14.5 mm/s at 325 °C and 350 °C and 3 mm/s at 400 °C. On the basis of the pressure limit and cracking limit, a safe extrusion processing zone is established, in which a high-quality extruded material having an elongation higher than 10% can be produced without hot cracking and internal cracking. All the extruded materials fabricated under the extrusion conditions lying within this safe zone have a completely recrystallized grain structure, and their grain size increases with increasing extrusion temperature and ram speed. However, the degree of this increase in grain size is fairly small because the undissolved particle stingers arranged parallel to the ED inhibit further growth of the recrystallized grains. At a given extrusion temperature, the tensile strength of the extruded material gradually decreases with increasing ram speed, which is attributed mainly to the weakening of the grain-boundary hardening effect through the grain coarsening. The grain size of the extruded material does not show any relationship with the *Z* value, which is considered a comprehensive process parameter, but its strength is inversely proportional to the logarithm of the *Z* value, which is expressed as $YS = -31.2 \cdot \log(Z) + 536$. Although the safe extrusion process conditions vary with various extrusion variables (e.g., the billet size, load capacity of an extruder, shape of extruded products, extrusion ratio, and lubrication condition), the extrusion limit diagram and the YS-*Z* relationship derived in this study will be of great help in designing the initial extrusion process conditions of the recently developed AZXWMM91100 alloy and predicting the mechanical strength of its extruded products.

Declaration of Competing Interest

The authors declare that they have no conflict of interest.

Acknowledgments

This research was supported by the National Research Foundation of Korea (NRF) grant funded by the Ministry of Science, ICT and Future Planning (MSIP, South Korea) (No. 2019R1A2C1085272) and by the R&D Center for Valuable Recycling (Global-Top R&BD Program) of the Ministry of Environment of Korea (No. 2016002220003).

References

[1] B.L. Mordike, T. Ebert, Mater. Sci. Eng. A 302 (2001) 37–45.
[2] M.E. Turan, H. Zengin, Y. Sun, Met. Mater. Int. 26 (2020) 541–550.
[3] J. Go, J.U. Lee, B.G. Moon, J. Yoon, S.H. Park, Met. Mater. Int. 26 (2020) 1779–1785.
[4] H.J.T. Ellingham, J. Soc. Chem. Ind. 63 (1944) 125–133.
[5] Y.M. Kim, C.D. Yim, H.S. Kim, B.S. You, Scr. Mater. 65 (2011) 958–961.
[6] S.H. Ha, J.K. Lee, S.K. Kim, Mater. Trans. 49 (2008) 1081–1083.
[7] G.L. Song, A. Atrens, Adv. Eng. Mater. 1 (1999) 11–33.
[8] B.S. You, Y.M. Kim, C.D. Yim, H.S. Kim, Magnesium Technology 2014, in: Magnesium Technology 2014, John Wiley & Sons Inc., Hoboken, New Jersey, 2014, pp. 325–329.
[9] S.K. Woo, C. Blawert, K.A. Yasakau, S. Yi, N. Scharnagl, B.C. Suh, Y.M. Kim, B.S. You, C.D. Yim, Corros. Sci. 166 (2020) 108451.
[10] Y.M. Kim, B.S. You, M.S. Shim, N.J. Kim, Magnesium Technology 2012, in: Magnesium Technology 2012, John Wiley & Sons Inc., Hoboken, New Jersey, 2012, pp. 217–219.
[11] Y. Go, S.M. Jo, S.H. Park, H.S. Kim, B.S. You, Y.M. Kim, J. Alloy. Compd. 739 (2018) 69–76.
[12] S.M. Baek, J.S. Kang, H.J. Shin, C.D. Yim, B.S. You, H.Y. Ha, S.S. Park, Corros. Sci. 118 (2017) 227–232.
[13] N. Papenberg, S. Gneiger, Mater. Sci. Forum 918 (2018) 28–33.
[14] S.H. Kim, S.W. Bae, S.W. Lee, B.G. Moon, H.S. Kim, Y.M. Kim, J. Yoon, S.H. Park, Mater. Sci. Eng. A 725 (2018) 309–318.
[15] S.H. Kim, S.W. Lee, B.G. Moon, H.S. Kim, Y.M. Kim, S.H. Park, J. Mater. Res. Technol. 8 (2019) 5254–5270.
[16] S. Gneiger, N. Papenberg, S. Frank, R. Gradinger, Magnesium Technology 2018, in: Magnesium Technology 2018, Springer International Publishing, Germany, 2018, pp. 105–113.
[17] W.A. Backofen, Metall. Trans. 4 (1973) 2679–2699.
[18] T. Lee, M. Yamasaki, Y. Kawamura, J. Go, S.H. Park, Met. Mater. Int. 25 (2019) 372–380.
[19] C. Bettles, M. Barnett, Advances in wrought Mg alloys: Fundamentals of Processing, Properties and Applications, 1st ed., Woodhead Publishing, Cambridge, 2012.
[20] D.L. Atwell, M.R. Barnett, Metall. Mater. Trans. A 38 (2007) 3032–3041.
[21] S.H. Kim, J.U. Lee, Y.J. Kim, B.G. Moon, B.S. You, H.S. Kim, S.H. Park, Mater. Sci. Eng. A 703 (2017) 1–8.
[22] T. Nakata, T. Mezaki, R. Ajima, C. Xu, K. Oh-ishi, K. Shimizu, S. Hanaki, T.T. Sasaki, K. Hono, S. Kamado, Scr. Mater. 101 (2015) 28–31.
[23] M.G. Jiang, C. Xu, T. Nakata, H. Yan, R.S. Chen, S. Kamado, Mater. Sci. Eng. A 667 (2016) 233–239.
[24] H.J. Kim, S.H. Kim, S.W. Lee, B.G. Moon, Y.M. Kim, J.H. Lee, J. Yoon, H. Yu, S.H. Park, Met. Mater. Int. 27 (2021) 514–521.
[25] G.E. Dieter, Mechanical Metallurgy, 3rd ed., McGraw-Hill, New York, 1986.
[26] V. DePierre, J. Lubr, J. Lubr. Technol 92 (1970) 398–405.
[27] T. Kunimine, N. Takata, N. Tsuji, T. Fujii, M. Kato, S. Onaka, Mater. Trans. 50 (2009) 64–69.
[28] D.H. Lee, B.G. Moon, Y.M. Kim, S.H. Park, J. Alloy. Compd. 862 (2021) 158051.
[29] J.U. Lee, S.H. Kim, Y.J. Kim, S.H. Park, Mater. Sci. Eng. A 714 (2018) 49–58.
[30] D.A. Porter, K.E. Easterling, Phase Transformations in Metals and Alloys, 2nd ed., Chapman & Hall, London, 1992.
[31] Z. Wang, F. Wang, Y. Peng, Y. Han, Nat. Commun. 6 (2015) 6942.
[32] D.H. Lee, S.H. Kim, H.J. Kim, B.G. Moon, Y.M. Kim, S.H. Park, Met. Mater. Int. 27 (2021) 530–537.
[33] L. Chen, M. Liang, G. Zhao, J. Zhou, C. Zhang, Vacuum 150 (2018) 136–143.
[34] L. Chen, S. Li, X. Chu, G. Zhao, J. Gao, Mater. Lett. 241 (2019) 104–107.
[35] N.V.R. Kumar, J.J. Blandin, C. Desrayaud, F. Montheillet, M. Suéry, Mater. Sci. Eng. A 359 (2003) 150–157.
[36] J. Bohlen, S. Yi, D. Letizg, K.U. Kainer, Mater. Sci. Eng. A 527 (2010) 7092–7098.
[37] J. Li, A. Zhang, H. Pan, Y. Ren, Z. Zeng, Q. Huang, C. Yang, L. Ma, G. Qin, J. Magnes. Alloy. 9 (2021) 1297–1303.
[38] S.H. Park, B.S. You, R.K. Mishra, A.K. Sachdev, Mater. Sci. Eng. A 598 (2014) 396–406.
[39] S.H. Park, H.S. Kim, B.S. You, Met. Mater. Int. 20 (2014) 291–296.
[40] S.H. Park, H.S. Kim, B.S. You, Mater. Sci. Eng. A 625 (2015) 369–373.
[41] H. Yu, S.H. Park, B.S. You, Y.M. Kim, H.S. Yu, S.S. Park, Mater. Sci. Eng. A 583 (2013) 25–35.
[42] R. Armstrong, I. Codd, R.M. Douthwaite, N.J. Petch, Philos. Mag. 7 (1962) 45–58.
[43] S.H. Kim, S.W. Lee, B.G. Moon, H.S. Kim, S.H. Park, J. Mater. Sci. Technol. 46 (2020) 225–236.
[44] H. Fu, B. Dönges, U. Krupp, U. Pietsch, C.P. Fritzen, X. Yun, H.J. Christ, Acta Mater. 199 (2020) 278–287.
[45] Y. Chen, Q. Wang, J. Peng, C. Zhai, W. Ding, J. Mater. Process. Technol. 182 (2007) 281–285.
[46] P. Feltham, Met. Treat. 23 (1956) 440–444.
[47] A. Mwembela, E.B. Konopleva, H.J. McQueen, Scr. Mater. 37 (1997) 1789–1795.
[48] S. Spigarelli, M. Cabibbo, E. Evangelista, M. Talianker, V. Ezersky, Mater. Sci. Eng. A 289 (2000) 172–181.
[49] H.J. McQueen, N.D. Ryan, Mater. Sci. Eng. A 322 (2002) 43–63.
[50] J.J. Jonas, C.M. Sellars, W.J.McG. Tegart, Metall. Rev. 130 (1969) 1–24.
[51] H. Mirzadeh, J. Magnes. Alloy. 2 (2014) 225–229.
[52] H. Mirzadeh, J. Mater. Res. Technol. 5 (2016) 1–4.
[53] H. Mirzadeh, J. Mater. Eng. Perform. 24 (2015) 1095–1099.
[54] H. Mirzadeh, J.M. Cabrera, A. Najafizadeh, Acta Mater. 59 (2011) 6441–6448.
[55] J. Wang, Z. Wu, S. Gao, R. Lu, D. Qin, W. Yang, F. Pan, J. Magnes. Alloy. 3 (2015) 79–85.
[56] W.L. Cheng, H.S. Kim, B.S. You, B.H. Koo, S.S. Park, Mater. Lett. 65 (2011) 1525–1527.